Enhanced photovoltaic performance of nanocrystalline CdTe/ZnO solar cells using sol-gel ZnO and positive bias treatment

B. I. MacDonald,[1,2] E. Della Gaspera,[1] S. E. Watkins,[1] P. Mulvaney,[2] and J. J. Jasieniak[1,a)]
[1]*CSIRO Materials Science and Engineering, Bayview Avenue, Clayton, Victoria 3168, Australia*
[2]*School of Chemistry and Bio21 Institute, The University of Melbourne, Parkville, Victoria 3010, Australia*

(Received 11 December 2013; accepted 26 April 2014; published online 8 May 2014)

The effect of doping and porosity of the n-type ZnO layer on the performance of solution-processed, sintered p-CdTe/n-ZnO nanocrystal photovoltaic (PV) devices is investigated. Amorphous sol-gel ZnO is found to be the best candidate with overall energy conversion efficiencies above 8% obtained if the ZnO is also indium doped. We demonstrate that when such PV devices are left under forward bias (in dark or light), the device efficiency values are raised to at least 9.8%, due to a substantially increased open-circuit voltage and fill-factor. This drastic enhancement is attributed to improved band alignment at the ITO/CdTe interface. The forward-bias treatment is slowly reversed over a period of days to weeks on standing under open circuit conditions, but is readily restored with further voltage treatment. The moderate processing conditions and high efficiency of such devices demonstrate that nanocrystal-based systems are a promising technology for photovoltaics. © *2014 AIP Publishing LLC*. [http://dx.doi.org/10.1063/1.4875381]

I. INTRODUCTION

Photovoltaic (PV) devices based on sintered nanocrystalline materials combine the affordability of solution-processing with the robustness of bulk inorganic semiconductors.[1,2] In order for these devices to achieve commercial relevance, it is crucial that their power conversion efficiencies (PCE) approach values similar to those of solar cells produced through traditional, vacuum-based deposition methods.[3] Recently, cadmium telluride (CdTe) nanocrystal based solar cells with efficiencies up to 7.3% have been obtained,[4] while efficiencies as high as 12.0% and 8.4% have been reported for devices using the more complex semiconductor materials, chalcopyrite (CIGSSe)[5] and kesterite (CZTGeSSe)[6] as absorber layers, respectively. Using a separate but related approach, IBM researchers have obtained efficiencies of 15.2% for CIGS[7] and 12.6% for CZTSSe[8] devices based on molecular precursors dissolved in hydrazine. Importantly, these chemically processed devices employ planar junctions for charge carrier separation and, in contrast to dye sensitized solar cell (DSSC) systems, do not employ a solvent. Crucially, the efficiency for the CIGS device is the highest of any deposition method to date—truly highlighting the potential of solution-processing as a cost-effective approach for the fabrication of photovoltaic devices.

CdTe solar cells that are prepared via close-space sublimation are currently one of the cheapest, commercially available photovoltaic technologies at a price point of ~$0.7 US/W with a maximum reported solar conversion efficiency of 19.6%.[9] These values demonstrate that CdTe is a viable material for low-cost solar cells. Deposition from nanocrystal inks can be optimized by judicious use of different particle morphologies. This has been exploited for CdTe devices by Gur *et al.*, who sintered CdTe and CdSe nanorods to form a bilayer donor/acceptor CdTe/CdSe junction and obtained efficiencies of 2.9%.[1] By removing the CdSe layer and using a simple device stack of ITO/CdTe/Al, Olson *et al.* attained conversion efficiencies of 5%.[10] It was proposed that the driving mechanism for charge separation and collection in this device was the Schottky junction formed at the CdTe/Al interface. Ultimately, the instability of this junction motivated us to use a highly n-doped ZnO window layer fabricated from spherical zinc oxide (ZnO) nanocrystals. Utilizing Mott-Schottky analysis, we showed that the depleted heterojunction of this inverted superstrate device architecture yields very high internal quantum efficiencies (>90%) and overall device performances that exceed 7%.[11]

While nanocrystal inks offer an exciting new approach to harnessing solar energy, a number of key challenges remain—understanding their bulk and interfacial properties, developing appropriate surface chemistry, and controlling the doping density in the annealed semiconductor films. Here, we focus on modifying the nature of the n-type contact with the lightly doped p-CdTe layer in a standard ITO/CdTe/ZnO/Al device structure. We show that sol-gel synthesis provides an alternative wet-chemical route for film deposition, which enables us to fabricate smooth interfaces between the ZnO and CdTe layers. Furthermore, we demonstrate that controlled doping of the n-type ZnO layer with indium leads to drastic enhancements in overall efficiency.

II. EXPERIMENTAL PROCEDURES

Solar cells were fabricated using a layer-by-layer assembly method outlined in Fig. 1 and described in detail elsewhere.[11] Briefly, CdTe layers were deposited from pyridine passivated CdTe nanocrystals of ~5 nm diameter that were dispersed in 1:1 1-propanol:pyridine. Following the deposition of each CdTe layer by spin-coating, the substrate was dipped into a saturated solution of $CdCl_2$ in methanol at

a)Author to whom correspondence should be addressed. Electronic mail: Jacek.Jasieniak@csiro.au.

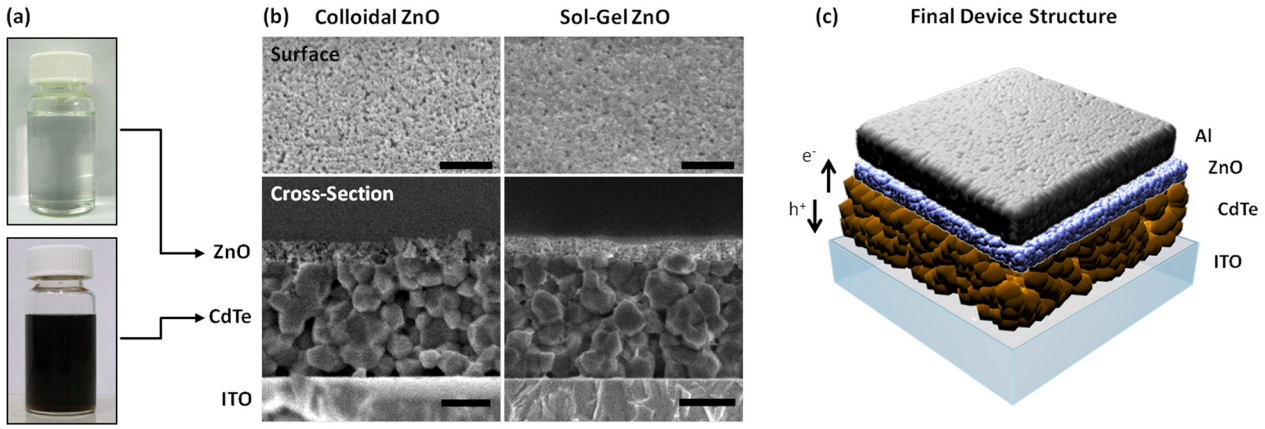

FIG. 1. (a) Typical nanocrystal dispersions used to deposit the individual layers of our sintered nanocrystal solar cells. (b) Representative SEM images of the surface and cross-section of ITO/CdTe/ZnO multi-layer films. In these samples, four layers of CdTe had been deposited with intermediate $CdCl_2$ and 350 °C treatment steps prior to the deposition of colloidal or sol-gel ZnO. Scale bars are 200 nm. (c) The final solar cell device architecture used for our studies.

60 °C for 10 s, rinsed with 1-propanol, dried under a nitrogen stream, and then annealed at 350 °C for 30 s in air to promote large-scale grain growth. This process was repeated a total of four times, resulting in a total CdTe thickness of ~400 nm. A ~60 nm thick n-type layer consisting of either nanocrystalline or sol-gel based ZnO was then deposited by spin-coating and annealed at 300 °C and 200 °C, respectively, for 2 min. The nanocrystalline colloidal dispersions used in this step were prepared in 1-propanol using the same methods previously reported.[12] Sol-gel ZnO was prepared by heating zinc acetylacetonate in 2-methoxyethanol and ethanolamine ([Zn] = 0.18 M, [Zn]/[Ethanolamine] = 1) at 60 °C for 2 h.[13] Indium doped sol-gel ZnO (InZnO) was prepared under analogous conditions, except a 2% mol/mol indium acetylacetonate solution was added to the zinc acetylacetonate precursor. Characteristic SEM images of these multi-layered structures are shown in Fig. 1(b). The devices were completed by thermal evaporation of an aluminium back contact, resulting in a final device structure: ITO/CdTe (400 nm)/ZnO (60 nm)/Al (100 nm) (Fig. 1(c)) with an active area of 0.2 ± 0.01 cm^2. Device testing was performed under 100 mW/cm^2 AM 1.5 conditions with all final device performances corrected for spectral mismatch.

III. RESULTS AND DISCUSSION

A. Sol-gel vs colloidal nanocrystalline ZnO

We first consider the electronic structure and composition of the various materials studied here. In our previous work, we utilized (i) photoelectron spectroscopy in air (PESA) to determine the CdTe ionization energy, (ii) Mott-Schottky analysis to determine doping densities, and (iii) literature energy level values for ZnO to approximate the flat-band potentials. Here, we provide a more detailed assessment of the electronic structure of each layer in the above devices, based on ultraviolet photoelectron spectroscopy (UPS) measurements (Fig. 2, Table I). In order to determine the conduction band edge values, we added the sum of the optical bandgap and the exciton binding energy (10 meV for CdTe and 60 meV for ZnO) to the UPS determined valence band energy.

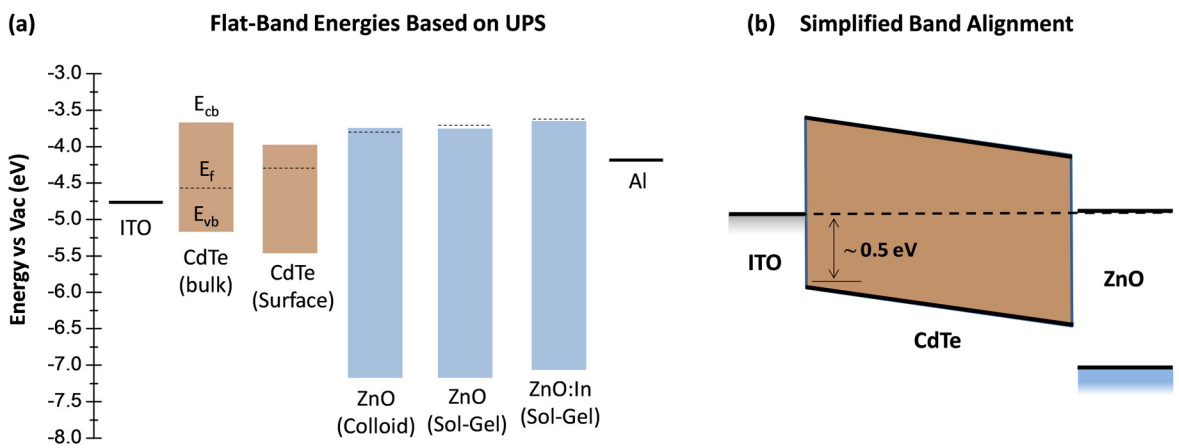

FIG. 2. (a) A schematic diagram of the flat-band energies derived for the various layers in our sintered solar cells. The bulk CdTe values are representative of the etched samples. To determine the conduction band energies (E_{vb}), we added the optical band gap and the exciton binding energy to the determined valence band energy (E_{vb}). The Fermi energies (E_f) for the CdTe and ZnO samples are included as dashed lines. (b) A simplified depiction of the band-alignment based on UPS and absorption measurements. This schematic ignores any band-bending at the contacts and only considers the case when the oxide and chloride species at the cathode act to deplete the majority carriers from the CdTe.

TABLE I. Summary of the UPS data of CdTe and the various ZnO thin films employed here as n-type window layers.

Sample	Secondary cut-off (eV)	E_v vs E_f (eV)	E_v vs vac (eV)	E_f vs vac (eV)	$E_{g,opt}$ (eV)	$E_{g,elec}$[a] (eV)	E_{cb} vs vac (eV)
CdTe surface	16.9	−1.14	−5.44	−4.30	1.45	1.46	−3.99
CdTe bulk	16.68	−0.58	−5.10	−4.52	1.45	1.46	−3.64
ZnO NC	17.4	−3.34	−7.14	−3.80	3.38	3.44	−3.76
ZnO SG	17.49	−3.44	−7.15	−3.71	3.36	3.42	−3.79
InZnO SG	17.58	−3.48	−7.10	−3.62	3.37	3.43	−3.67

[a]Calculated as the sum of the optical bandgap, derived from optical absorption measurements, and the bulk exciton binding energy, 10 meV for CdTe and 60 meV for ZnO.

Each of the ZnO layers that we trialed here showed highly n-type behavior, with the In doped samples exhibiting slightly more positive Fermi energies with respect to vacuum. The $CdCl_2$ treated and thermally annealed CdTe layers exhibited a low Fermi energy of −4.3 eV, characteristic of an n-type CdTe surface. This contrasts with the known p-type conductivity of bulk CdTe. XPS measurements of these surfaces indicated a Cd/Te ratio at the surface of ∼1.5, as well as excessive levels of chlorine (54%) and oxygen (55%) relative to the sum of Cd and Te atomic signals. This suggests that the surface was contaminated by excess $CdCl_2$ and various cadmium oxide species. Such contaminants are typical for $CdCl_2$ and air treated, non-solution processed CdTe films, and these layers must be removed via etching to achieve Ohmic contacts to CdTe in conventional superstrate devices.[14] Here, the surfaces were etched back by dipping the samples in dilute HCl (pH ∼ 4) for 30 s, rinsing with deionized water then drying under N_2 flow. This treatment resulted in a drastic reduction of the Cd/Te ratio to ∼0.9, as well as decreases of the chlorine and oxygen signals to 32% and 10% relative to the sum of Cd and Te, respectively. UPS measurements of this etched surface showed it to be weakly p-type, with a Fermi level ∼0.5 eV above the valence band. This implies that the doping densities must be ∼1–2 orders of magnitude lower (10^{14}–10^{15} cm^{-3}) than our previously predicted values (∼10^{16} cm^{-3}) based on a Mott-Schottky analysis of completed cells.[11] The impact of lower doping density on the band structure of CdTe within our devices is illustrated in Figure 2(b).

The implications of these findings are two-fold: (i) the chlorine and oxygen rich top surfaces (and any chemically similar surfaces surrounding the individual CdTe nanocrystals within the bulk) are likely to contribute to the depletion of the majority carrier (holes) in the CdTe and (ii) the nanocrystalline layer possesses comparable doping levels to those of bulk CdTe prepared via conventional vacuum based techniques.[15] Such low doping densities will result in depletion layer thicknesses of several microns, meaning that a "full depletion mechanism" operates in all of the CdTe/ZnO devices studied. This also explains why the short-circuit current density is not a strong function of the CdTe thickness in the sub-micron thickness range, as long as sufficient light absorption is achieved.[11]

Having shown that the CdTe layers possess low doping densities, with the surface being passivated by oxides and chlorides, we now examine the performance of the resulting CdTe-based sintered solar cells. The devices fabricated using ZnO nanocrystals exhibited a power conversion efficiency of 7.4% (Fig. 3(a), Table II), in line with our previously reported results for this device architecture.[4] The primary factors limiting the performance of these cells are the low open-circuit voltage and low fill factors (FFs) relative to vacuum-deposited CdTe solar cells of comparable thickness.[16]

Each of these factors can be related to the quality of the CdTe layer and its interface with the ITO and ZnO layers.[17] Here, we specifically examined the latter using ZnO layers based on low-temperature sol-gel chemistry. Such films are largely amorphous in nature at temperatures up to ∼200 °C, which eliminates the presence of grain boundaries and allows for a more conformal coating on top of the underlying CdTe.[18] In addition, sol-gel processing also allows the easy incorporation of dopants into the precursor solution.[19] This is in stark contrast to ZnO nanocrystals, for which controlled extrinsic doping is notoriously difficult to achieve.[20] Solar cells fabricated using sol-gel ZnO and InZnO layers with the inverted superstrate structure exhibited photoconversion efficiencies of 7.8% and 8.0%, respectively—a modest improvement over devices containing nanocrystalline ZnO.

The primary reasons for the efficiency boosts in the sol-gel devices are (i) improved open-circuit voltage (V_{oc}) and (ii) higher FF. Each of these factors can be explained by a higher built-in field in the devices stemming from the less negative Fermi energies vs vacuum of the sol-gel layers, in particular, that of the InZnO (see Table I), and/or

TABLE II. Performance characteristics of ITO/CdTe(400 nm)/ZnO(60 nm)/Al solar cells with different types of ZnO under AM 1.5 illumination. All values have been corrected for spectral mismatch.

ZnO type	J_{sc} (mA/cm^2)	V_{oc} (V)	FF (%)	PCE (%)	Rs (Ω cm^2)	Rsh (kΩ cm^2)
Nanocrystal	22.3	0.56	59	7.4	4.9	0.4
Sol-gel	21.9	0.59	60	7.8	4.1	0.3
Sol-gel In doped	20.9	0.61	63	8.0	4.4	1.1
Sol-gel In doped (bias treated)	21.2	0.69	67	9.8	4.3	1.7

reduced recombination stemming from the CdTe/ZnO interface. Inspection of the interface between CdTe and sol-gel deposited ZnO (see Fig. 1(b)), indeed shows that the sol-gel ZnO films are denser than the nanocrystalline ZnO films and form a more conformal interface with the CdTe layer. Both of these structural factors are likely to benefit charge collection across this interface. In terms of shunt resistance (R_{sh}), the undoped sol-gel ZnO performs slightly worse than the nanocrystalline layer, while the InZnO exhibits a nearly three-fold higher R_{sh} value of 1.1 kΩ cm^2. The impact of this enhanced R_{sh} can be clearly observed in the dark J-V measurements presented in Fig. 3(b). It is unlikely that this improvement is related to the electrical properties of the InZnO itself, as the reported values for doping density (10^{18}–10^{19} cm^{-3}) and electron mobility ($\sim 10^{-3}$ cm^2 V^{-1} s^{-1})[12,16] are similar for all three types of ZnO studied here. Instead, we believe the indium is likely interacting with the CdTe surface, passivating or compensating existing trap states and thereby reducing losses stemming from Shockley-Read-Hall recombination.[21]

B. Forward bias treatments

An unusual effect of "charging" the device, by means of a forward bias treatment, was observed with these PV devices. To the best of our knowledge, this phenomenon has not been reported previously (During the review process for this manuscript, it came to our attention that a similar finding had been reported elsewhere by Panthani *et al.*[22] Further information on such device behavior can also be found in Ref. 23). The above solar cell devices were tested over a limited voltage range between −1 V and +1 V. It was observed that under these conditions the solar cells exhibited little change in device behavior upon repeated voltage sweeps at a rate of <50 mV/s). However, when the devices were held under a larger forward bias, (both in the light and dark), drastic improvements in device performance were observed (see Table III). We found that the best performance was obtained when the devices were held at a bias of +3 V, which corresponded to a (dark) current density within the cells of 1.3–1.8 A/cm^2. In Fig. 4(a), we present the J-V curves for a CdTe/InZnO device treated at a +3 V bias for varying lengths of time. The application of such a voltage treatment led to a steady increase in both open-circuit voltage and fill-factor, reaching respective maximum values of 0.69 V and 0.67 following 240 s of bias-treatment. We also observed a further increase in shunt resistance to 1.7 kΩ cm^2. Beyond this time, little further change in device performance was observed. These enhancements in device characteristics led to a power conversion efficiency of 9.8%, one of the highest reported to date for CdTe-based nanocrystal solar cells (Table II).

The result of this forward biasing treatment is a metastable device state. We observed that following biasing, the device efficiency remained nearly constant over several days when stored under open-circuit conditions and ambient room lighting, then gradually decayed back to the initial level (or even lower). However, the enhanced efficiency could be readily restored by re-application of the forward bias treatment. Shown in Fig. 4(b) is the J-V curve of an encapsulated, bias treated device after 6 months of storage under ambient conditions. While the J_{sc} value and fill factor had decreased only slightly after this extended storage, the open-circuit voltage had dropped to 0.50 V, resulting in an efficiency of 6.0%. Once the device was re-treated at +3 V for 240 s, performance was restored to a PCE of 9.4% (Fig. 4(b)).

In order to determine whether the nature of the n-type charge transport layer was responsible for such behavior, we assessed the effect of bias treatment on both sol-gel and nanocrystalline ZnO based CdTe devices. In both cases, the same relative improvement in efficiency was observed. Additionally, we fabricated Schottky-type devices with an ITO/CdTe/Al structure, i.e., with no ZnO layer. Such Schottky cells exhibited similar performance improvements upon bias treatment, with efficiencies plateauing at ∼7.8%. These observations clearly indicate that modifications at the photo-anode interface are not responsible for the changes in device efficiency.

Whilst the definitive cause of this effect is at present unclear, the above findings indicate that the voltage

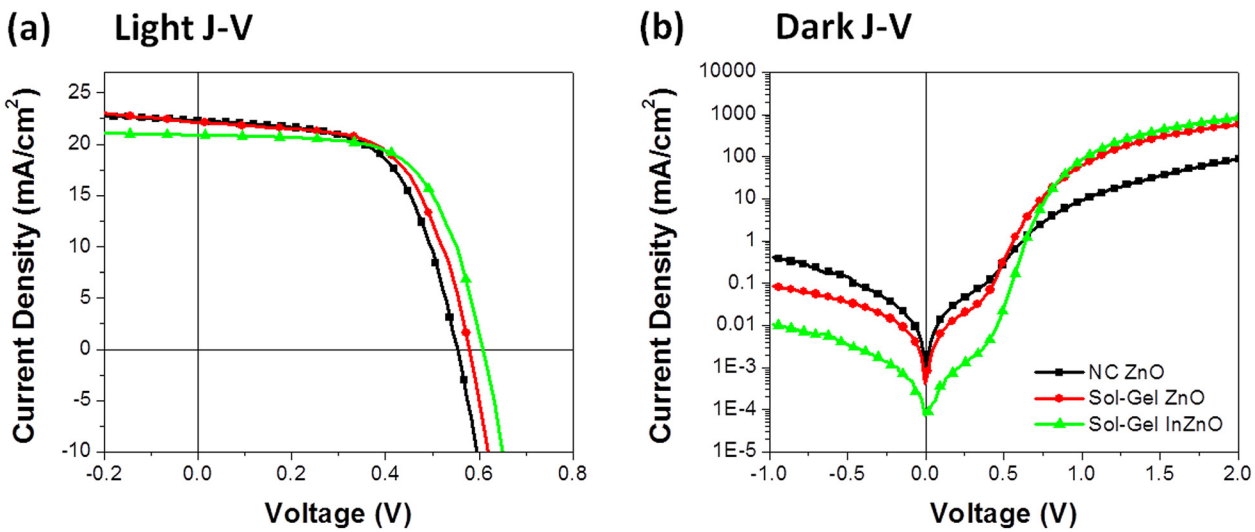

FIG. 3. (a) Current-voltage curves for ITO/CdTe(400 nm)/ZnO(60 nm)/Al solar cells made using nanocrystalline ZnO (black, squares), sol-gel ZnO (red, circles), and sol-gel InZnO (green, triangles). (b) Semi-log plot of dark current density versus voltage for the same devices.

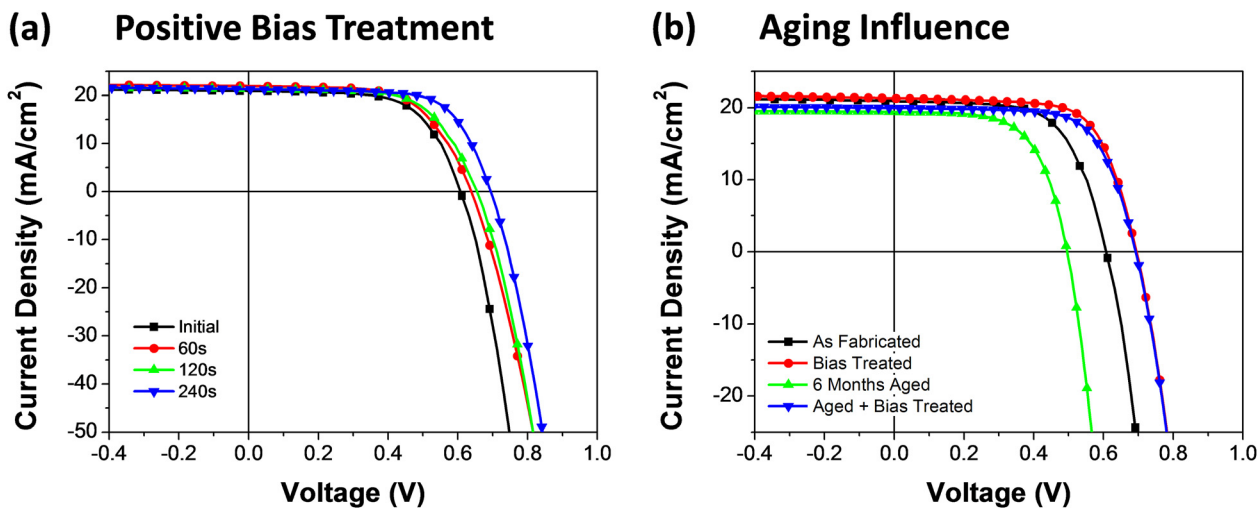

FIG. 4. (a) Current-voltage curves for ITO/CdTe/InZnO/Al solar cells held at a positive bias of +3 V for varying lengths of time prior to initiating the J-V sweep. (b) A comparison of the current-voltage curves of an encapsulated device that was initially prepared and positive bias treated to that stored in air for 6 months before and after a +3 V re-treatment for 240 s.

treatment is modifying the electronic structure within the cadmium telluride layer and/or at the interface between the nanocrystalline CdTe and the ITO electrode. Based on the energy level offset at the ITO/CdTe interface (Fig. 2(a)), as well as the low doping density of the CdTe layers (see above), a non-Ohmic contact is likely. Indeed, this is one of the primary reasons that the open-circuit voltage and, therefore, device efficiency of our cells is limited relative to conventional CdTe solar cells.[24] The significant enhancement of both V_{oc} and the fill factor in the devices following the bias treatment is consistent with an improved band alignment and a minimized injection barrier at the photo-anode. By applying a forward bias and, therefore, injecting a high density of both electrons and holes into the device, shallow and deep surface traps in the CdTe layer and at the electrode interfaces will be filled. This must act to modify the CdTe grain boundary depletion characteristics[25] or to create a favorable dipole layer at the ITO/CdTe interface,[26] respectively. Because we see limited changes in device performance following extended illumination under short-circuit conditions and only observe this "charging" behavior at high positive potentials, the filling of traps within the bulk of the CdTe layer is likely to play a lesser role than the interface between the ITO/CdTe.

In addition to mobile carrier induced modifications of this interface, another equally viable explanation for such behavior is electric field driven ionic migration, with copper based species being a potential source. For example, the Cu_{Cd} acceptor, which is negatively charged relative to the CdTe lattice, is commonly found in high performing CdTe cells.[27] Under positive bias, the Cu will migrate toward the ITO/CdTe contact, where it has been previously shown that the presence of Cu can lead to improved device performance.[28,29] Once the bias is removed from the device, the charged species will diffuse back into the bulk of the CdTe layer, consistent with the reversible performance behavior observed in our devices. The route by which Cu, or an alternative dopant, could be introduced into our devices is not currently known, although impurities in either the CdO nanocrystal precursor or the $CdCl_2$ solution used to promote crystal growth upon sintering are the most likely sources. Despite the current uncertainty, it is evident that if the photovoltaic devices could be stabilized in the "charged" state, then CdTe/ZnO nanocrystal solar cells would provide a truly cost-effective alternative to DSSC and organic photovoltaic structures.

TABLE III. Performance characteristics of ITO/CdTe(400 nm)/ZnO(60 nm)/Al solar cells treated at +3 V for varying lengths of time prior to the J-V sweep. All values were recorded under AM 1.5 illumination and have been corrected for spectral mismatch.

Postproduction treatment time (s)	J_{sc} (mA/cm^2)	V_{oc} (V)	FF (%)	PCE (%)
0	20.9	0.61	63	8.0
60	21.8	0.64	61	8.5
120	22.0	0.67	62	9.1
240	21.2	0.69	67	9.8

IV. CONCLUSIONS

We have compared colloidal and sol-gel routes for the formation of the n-type ZnO layer in sintered p-CdTe nanocrystal solar cells. The optimal device efficiency was achieved when sol-gel derived indium doped ZnO was used. While this highlights the importance of optimizing the n-type charge transport material, the performance of all studied devices could be further increased by "charging" the device through a forward biasing treatment, applied post-production. Such a treatment enhanced the open-circuit voltage and fill factor of the device, allowing efficiencies to increase from 7.4% to 9.8% for the CdTe/InZnO architecture. At this point, the "charging" phenomenon is thought to be related to the accumulation of charge at the ITO/CdTe interface and/or electric field driven ion migration. Further investigations into the precise origin of this phenomenon are required to stabilize the performance of these solution-processed devices at such high efficiencies.

ACKNOWLEDGMENTS

B.I.M. wishes to acknowledge the University of Melbourne for MIFRS and MRS scholarships and CSIRO for a Ph.D. studentship. This work was funded through the Flexible Electronics Theme of the CSIRO Future Manufacturing Flagship, the Australian Renewable Energy Agency through the Australian Centre for Advanced Photovoltaics and through the ARC Grant No. DP110105341 awarded to J.J.J. P.M. acknowledges support through ARC Grant Nos. DP 0985325 and 130102134.

[1]I. Gur, N. A. Fromer, M. L. Geier, and A. P. Alivisatos, Science **310**(5747), 462 (2005).
[2]Q. Guo, H. W. Hillhouse, and R. Agrawal, J. Am. Chem. Soc. **131**(33), 11672 (2009).
[3]T. Aramoto, S. Kumazawa, H. Higuchi, T. Arita, S. Shibutani, T. Nishio, J. Nakajima, M. Tsuji, A. Hanafusa, T. Hibino, K. Omura, H. Ohyama, and M. Murozono, Jpn. J. Appl. Phys., Part 1 **36**(10), 6304 (1997).
[4]B. I. MacDonald, A. Martucci, S. Rubanov, S. E. Watkins, P. Mulvaney, and J. J. Jasieniak, ACS Nano **6**(7), 5995 (2012).
[5]Q. J. Guo, G. M. Ford, R. Agrawal, and H. W. Hillhouse, Prog. Photovoltaics **21**(1), 64 (2013).
[6]Q. J. Guo, G. M. Ford, W. C. Yang, C. J. Hages, H. W. Hillhouse, and R. Agrawal, Sol. Energy Mater. Sol. Cells **105**, 132 (2012).
[7]T. K. Todorov, O. Gunawan, T. Gokmen, and D. B. Mitzi, Prog. Photovoltaics **21**(1), 82 (2013).
[8]W. Wang, M. T. Winkler, O. Gunawan, T. Gokmen, T. K. Todorov, Y. Zhu, and D. B. Mitzi, "Device characteristics of CZTSSe thin-film solar cells with 12.6% efficiency," Adv. Energy Mater. (published online).
[9]M. A. Green, K. Emery, Y. Hishikawa, W. Warta, and E. D. Dunlop, Prog. Photovolt: Res. Appl. **21**, 827–837 (2013).
[10]J. D. Olson, Y. W. Rodriguez, L. D. Yang, G. B. Alers, and S. A. Carter, Appl. Phys. Lett. **96**(24), 242103 (2010).
[11]J. Jasieniak, B. I. MacDonald, S. E. Watkins, and P. Mulvaney, Nano Lett. **11**(7), 2856 (2011).
[12]A. Wood, M. Giersig, M. Hilgendorff, A. Vilas-Campos, L. M. Liz-Marzan, and P. Mulvaney, Aust. J. Chem. **56**(10), 1051 (2003).
[13]M. Ohyama, H. Kozuka, T. Yoko, and S. Sakka, J. Ceram. Soc. Jpn. **104**(4), 296 (1996).
[14]D. H. Rose, F. S. Hasoon, R. G. Dhere, D. S. Albin, R. M. Ribelin, X. S. Li, Y. Mahathongdy, T. A. Gessert, and P. Sheldon, Prog. Photovoltaics **7**(5), 331 (1999).
[15]B. E. McCandless and J. R. Sites, *Handbook of Photovoltaic Science and Engineering* (John Wiley & Sons, 2003).
[16]N. R. Paudel, K. A. Wieland, and A. D. Compaan, Sol. Energy Mater. Sol. Cells **105**, 109 (2012).
[17]B. A. Chambers, B. I. MacDonald, M. Ionescu, A. Deslandes, J. Quinton, J. J. Jasieniak, and G. Andersson, Sol. Energy Mater. Sol. Cells **125**, 164 (2014).
[18]Y. M. Sun, J. H. Seo, C. J. Takacs, J. Seifter, and A. J. Heeger, Adv. Mater. **23**(14), 1679 (2011).
[19]E. J. Luna-Arredondo, A. Maldonado, R. Asomoza, D. R. Acosta, M. A. Melendez-Lira, and M. D. L. Olvera, Thin Solid Films **490**(2), 132 (2005).
[20]S. C. Erwin, L. J. Zu, M. I. Haftel, A. L. Efros, T. A. Kennedy, and D. J. Norris, Nature **436**(7047), 91 (2005).
[21]D. M. Oman, K. M. Dugan, J. L. Killian, V. Ceekala, C. S. Ferekides, and D. L. Morel, Sol. Energy Mater. Sol. Cells **58**(4), 361 (1999).
[22]M. G. Panthani, J. M. Kurley, R. W. Crisp, T. C. Dietz, T. Ezzyat, J. M. Luther, and D. V. Talapin, Nano Lett. **14**(2), 670 (2014).
[23]B. I. MacDonald, Ph.D. thesis, University of Melbourne, 2013.
[24]D. L. Batzner, A. Romeo, H. Zogg, R. Wendt, and A. N. Tiwari, Thin Solid Films **387**(1–2), 151 (2001).
[25]J. Nelson, *The Physics of Solar Cells* (Imperial College Press, 2003).
[26]F. Capasso, *Heterojunction Band Discontinuities: Physics and Device Applications* (Elsevier Science Publishing Co., 1987).
[27]J. Perrenoud, L. Kranz, C. Gretener, F. Pianezzi, S. Nishiwaki, S. Buecheler, and A. N. Tiwari, J. Appl. Phys. **114**(17), 174505 (2013).
[28]R. W. Birkmire, B. E. McCandless, and W. N. Shafarman, Sol. Cells **23**(1–2), 115 (1988).
[29]A. Romeo, G. Khrypunov, S. Galassini, H. Zogg, and A. N. Tiwari, Sol. Energy Mater. Sol. Cells **91**(15–16), 1388 (2007).